Original Paper

Viscosity of glass below the transformation temperature

Holger Meinhard, Wolfgang Fränzel and Peter Grau

Fachbereich Physik, Martin-Luther-Universität Halle-Wittenberg, Halle/Saale (Germany)

Glass is an ideally brittle material at room temperature. The results of hardness indentation tests demonstrate this property by crack formation at the corners of the indent. But it is possible to avoid the crack formation if the load, the contact area and the deformation rate, respectively, are small enough. The mechanisms of this permanent deformation of brittle glasses by indentation close to room temperature have not been understood completely up to now. Viscous flow is responsible for permanent deformation of glasses above the transformation temperature (T_g). The same mechanism of deformation during indentation experiments is assumed in this work hypothetically, taking into account the very high stresses (GPa range) in the local volume around the indenter tip. This hypothesis of deformation at room temperature will be verified by independent experiments that work like viscometers in principle (e.g. cylinder compression experiments, ball indentation experiments). All experiments were analysed with the help of simple rheological models. Additionally some ball indents were analysed by topographical investigations to get first hints of viscoelastic deformation behaviour below T_g of glass.

Viskosität von Glas unterhalb der Transformationstemperatur

Glas gilt bei Raumtemperatur als ideal sprödes Material. Bei Härteeindrücken äußert sich diese Sprödigkeit durch permanente Rißbildung an den Eindruckecken. Bei sehr kleinen Belastungen, Kontaktflächen bzw. Deformationsgeschwindigkeiten ist jedoch die Erzeugung bleibender und durchaus rißfreier Eindrücke auch in Gläsern möglich. Der dieser Verformung zugrundeliegende Mechanismus wird bisher nicht vollständig verstanden. Für Temperaturen oberhalb der Transformationstemperatur ist das viskose Fließen als Ursache für die Möglichkeit der Glasverformung unbestritten. Auch für die Indenterexperimente, bei denen lokal sehr hohe Spannungen (GPa-Bereich) in der Umgebung der Indenterspitze auftreten können, wird hier von diesem Mechanismus ausgegangen. Diese Viskositätshypothese für Verformungen bei Raumtemperatur soll mit unabhängigen Experimenten nach dem Prinzip der Viskosimeter überprüft werden (z.B. Zylinderstauchversuche, Kugeleindruckexperimente). In dieser Arbeit werden für alle Versuchstypen einfache rheologische Modelle zur Auswertung verwendet. Um erste Hinweise auf viskoelastisches Deformationsverhalten auch unterhalb T_g zu erhalten, wurden einige Kugeleindrücke zusätzlich topografisch untersucht.

1. Introduction

Glasses are considered as a brittle material below the transformation temperature (T_g). That means a macroscopic deformation experiment at room temperature is accompanied by immediate fraction if the Griffith stress is exceeded. In this respect the deformation behaviour is a purely elastic one. But it is also possible to deform glasses permanently without cracks by indentation experiments if the deformation rate is small enough. In 1933 Tammann [1] used conventional indentation experiments to study the viscosity of glasses but without defined loading rate. The indents were performed during increasing of the temperature step by step. Then that temperature was identified as the transformation temperature of the glass at which the indents are without cracks for the first time. In this view the deformation of glass during indentation at room temperature without cracks is considered as viscous. This interpretation diverges strongly from the general experience given by the dependence of the viscosity of glasses on temperature near T_g which is described by the equation of Vogel, Fulcher, and Tammann (VFT) [2 to 4]:

$$\lg \eta = A + \frac{B}{T - T_0} \tag{1}$$

where η is the viscosity at the temperature T, A and B are constants and T_0 is the so-called Vogel temperature. In accordance with equation (1) the viscosity will be infinite ($\eta \to \infty$) at T_0. For silicate glasses T_0 is many times higher than room temperature. Nevertheless, one can find viscosity values for room temperature in Frischat

Received 6 September 2000.

Presented in German at: 73rd Annual Meeting of the German Society of Glass Technology (DGG) in Halle/Saale (Germany) on 1 June 1999.

[5] (10^{20} Pa s) and Macosco [6] (10^{40} Pa s). That yields Maxwell relaxation times τ from 10^9 s (30 years) to 10^{29} s with

$$\tau = \frac{\eta}{E} \tag{2}$$

where E is the elastic modulus. These relaxation times have an incompatibly high level in comparison with the duration of indentation experiments amounting to about 100 s.

The hardness number represents the generation of very high contact stresses in a small volume around the indenter tip which never are reached by uniaxial compression or tension experiments. This special quality is an important peculiarity of the deformation of materials by indentation and may reduce the viscosity during indentation so that the relaxation times $\tau \approx 100$ s are in accordance with the duration of experiments. There are two conceivable reasons. First, a part of the added mechanical energy is converted into thermal energy following by an increase in temperature and a decrease in viscosity. A rough adiabatic estimation yields sufficiently high temperatures [7]. Second, a reduction of the viscosity under the very high pressure of an indentation experiment is conceivable. The consequences of these possible reasons were studied in a first step by topographical investigations of some ball indents performed at typical temperatures below T_g.

The indentation experiments to generate very high stresses only were obtained at room temperature for technical reasons with the help of a NanoIndenter®II (MTS Systems Corporation, Nano™ Instruments Innovation Centre, Oak Ridge, TN (USA)). For a higher temperature range from room temperature to T_g contact experiments were carried out which work like penetration viscometers in principle [8 and 9]. Furthermore, the well-known cylinder compression experiments working like a parallel plate viscometer were used [10] as standard and for comparison with ball indentation experiments at temperatures below T_g. To broaden the established experiments of Brückner and co-workers [11] a relaxation part was added to the loading part of each type of experiments in order to get more independent information about the time-dependent deformation process. All experiments were analysed using unified rheological principles. With respect to the different contact experiments the rheological models must be modified theoretically.

2. Theoretical

2.1 Cylinder compression experiments

The method of deformation of compact cylindrical glass samples is nearly the same as that using a parallel plate viscometer. A relation to calculate the viscosity η was given by Gent [10]:

$$\eta = \frac{F}{3\,\dot{l}\,V\left(\dfrac{1}{l^2(t)} + \dfrac{V}{2\pi\,l^5(t)}\right)} \tag{3}$$

where F is the loading force, $\dot{l}$ is the axial deformation rate, V is the volume of the sample and $l(t)$ is the actual length of the sample at the time t. During the deformation the volume of the sample is assumed to be constant

$$V = A_0\,l_0 = \pi r^2(t)\,l(t) \tag{4}$$

where r is the radius of the sample, l_0 is the length and A_0 is the cross section of the sample at the time $t = 0$. Only if the deformation is purely viscous, equation (3) is usable to calculate the viscosity η. For temperatures from T_g downward the viscosity increases to such high values that the flow rates cannot be realized by the practicable deformation rates of the testing system. Furthermore, elastic parts of deformation are not considered by equation (3). Therefore, the experimental data were analysed by rheological models, which include elastic, and viscous parts of deformation and, additionally, relaxation experiments after the loading part. Using a Zener-Maxwell standard model yields the following differential equation:

$$\dot{\sigma} + \frac{E_M}{\eta}\,\sigma = (E_M + E_H)\,\dot{\varepsilon} + \frac{E_M\,E_H}{\eta}\,\varepsilon \tag{5}$$

where σ is the stress, ε is the strain, E_M and E_H are the elastic parameters of the two Hookean elements, η is the viscosity parameter of the Newtonian element and the dotted symbols stand for the rates of the corresponding quantities. For the loading part with $\dot{\varepsilon} = \dot{\varepsilon}_c = \text{const}$ and $\varepsilon = \dot{\varepsilon}_c\,t$ the solution of equation (5) is

$$\sigma(t) = \dot{\varepsilon}_c\,\eta\left[1 - \exp\left(-\frac{E_M}{\eta}\,t\right)\right] + E_H\,\dot{\varepsilon}_c\,t\,, \quad t \le t_f \tag{6}$$

where t_f is the time of the end of the loading part. For the relaxation experiment with $\varepsilon = \varepsilon(t = t_f) = \varepsilon_f = \text{const}$ yields

$$\sigma(t) = \sigma_\infty + (\sigma_f - \sigma_\infty)\exp\left(-\frac{E_M}{\eta}\,(t - t_f)\right), \quad t > t_f \tag{7}$$

with $\sigma_f = \sigma(t = t_f)$ and $\sigma_\infty = E_H\,\varepsilon_f$.

For $E_H \to 0$ equation (5) stands for a pure Maxwell model which describes simple viscoelastic materials.

2.2 Indentation experiments with spherical indenter

The equation for the analysis of purely viscous deformation by indentation with spherical indenter was given by Douglas [8]:

$$\eta = \frac{9F\,t}{32\,\sqrt{2R}\,h^{3/2}}\,. \tag{8}$$

This type of test was realized by indentation creep experiment that corresponds with the principle of a penetration viscometer. To obtain more information a type of experiment was carried out with two parts, loading and relaxation, in the same manner as for uniaxial compression.

For purely elastic deformation by spherical indenter the relation between the loading force F and the indentation depth h_{el} was found by Hertz in 1881 [12]:

$$F = \frac{4}{3}\,E^*\,\sqrt{R}\,h_{el}^{3/2} \tag{9}$$

where R is the radius of the spherical indenter and E^* is the reduced elastic modulus resulted from $1/E^* = (1-\nu^2)/E + (1-\nu_i^2)/E_i$. Here E, ν and E_i, ν_i are the elastic modulus and the Poisson ratio of the sample and the indenter, respectively. For $E_i \gg E$ it is approximately

$$E^* \approx \frac{E}{1-\nu^2}\,. \tag{10}$$

So equation (9) can be written as

$$F = \frac{4}{3}\,\frac{E}{(1-\nu^2)}\,\sqrt{R}\,h_{el}^{3/2}\,. \tag{11}$$

The strain for deformation by spherical indenter is given in [13]:

$$\varepsilon = \Gamma\,\frac{a}{R} \tag{12}$$

where a is the radius of the contact area of the indent, R is the radius of the sphere and Γ is a numerical constant of the material and is given in [13] for metals to be $\Gamma \approx 0.2$. The relation between the indentation depth h and the contact radius a is given in [14] for viscoelastic materials as $a^2 = R\,h$. In accordance with equation (12) the relation between strain ε and indentation depth h is

$$\varepsilon = \Gamma\,\sqrt{\frac{h}{R}}\,. \tag{13}$$

For the strain rate, $\dot{\varepsilon}$ is yielded if $\dot{h} = \dot{h}_c = \text{const}$ and hence $h = \dot{h}_c\,t$

$$\dot{\varepsilon} = \frac{\Gamma}{2}\,\sqrt{\frac{\dot{h}_c}{R\,t}}\,. \tag{14}$$

To describe the deformation behaviour of viscoelastic materials, in [15] a solution to this problem is proposed by replacing the elastic constants in the solution to the associated elastic problem by viscoelastic functions. To analyse all types of deformation experiments by the same rheological model, the viscoelastic function $\psi(t)$ was derived from the Zener-Maxwell model in accordance with equation (6) for the loading part:

$$\psi(t) = \eta\,\dot{\varepsilon}_c\left[1-\exp\left(-\frac{E_M}{\eta}\,t\right)\right] + E_H\,\dot{\varepsilon}_c\,t\,. \tag{15}$$

If replacing $E \leftrightarrow \{m_s\,\Psi(t)\}$ in equation (11), where m_s is the geometric constant to verify the special kind of the deformation process ($m_s = 1$ for shear and $m_s = 3$ for tensile experiments [16]), the time dependence for the loading part of deformation by spherical indentation is given with respect to equation (14) by:

$$F(t) = \Gamma_s\,\dot{h}_c\left[\eta\left(1-\exp\left(-\frac{E_M}{\eta}\,t\right)\right)t + E_H\,t^2\right],\quad t \le t_f \tag{16}$$

with

$$\Gamma_s = \frac{2\Gamma\,m_s}{3(1-\nu^2)}\,. \tag{17}$$

Using the same principle for the relaxation part (see equation (7), but with $\dot{h}_c = 0$ and $h = h(t = t_f) = h_f = \text{const}$), for the time dependence of the drop in load

$$F(t) = F_\infty + (F_f - F_\infty)\exp\left(-\frac{E_M}{\eta}\,(t-t_f)\right),\quad t > t_f \tag{18}$$

is yielded, where $F_f = F(t = t_f)$ at the starting time of the relaxation experiment and $F_\infty = \frac{4}{3}\,E_H\,\sqrt{R}\,(\dot{h}_c\,t_f)^{3/2}$ in accordance with equation (9).

2.3 Nanoindentation experiments

To realize very high stresses during the contact compression process, it is reasonable to use a sharp indenter. In this work a Vickers diamond pyramid was used for nanoindentation experiments. Therefore, it was necessary to modify the elements of rheological model for the conditions of nanoindentation experiments. The methodology for modelling is the superposition of three parts of indentation depth: an elastic part h_{el}, a viscous part h_{fl} and a plastic part h_{pl}, respectively.

The relation between the loading force F and the part h_{el} for purely elastic deformation is given in [17 and 18]:

$$F = C_G\,E^*\,h_{el}^2 \tag{19}$$

where $C_G = 2.22$ is the numerical constant of the Vickers pyramid and the reduced modulus E^* is given by the argumentation following equation (9).

Table 1. Parts of indentation depth $h(t) = h_{el} + h_{fl} + h_{pl}$ in accordance with equations (19), (21) and (22) for the loading, holding and unloading part of nanoindentation experiments

part of nanoindentation experiment	indentation depth		
	elastic part h_{el}	viscous (flow) part h_{fl}	plastic part h_{pl}
loading part $F = \dot{F}_c\, t$ $t \leq t_f$	$\sqrt{\frac{\dot{F}_c\, t}{2.22\, E^*}}$	$\sqrt{\frac{\dot{F}_c\, t^2}{26.43\, \eta}}$	$\sqrt{\frac{\dot{F}_c\, t}{26.43\, H}}$
holding part $F = F_{max} = \dot{F}_c\, t_f$ $t_f < t \leq t_f + t_h$	$\sqrt{\frac{\dot{F}_c\, t_f}{2.22\, E^*}}$	$\sqrt{\frac{\dot{F}_c(2t_f\, t - t_f^2)}{26.43\, \eta}}$	$\sqrt{\frac{\dot{F}_c\, t_f}{26.43\, H}}$
unloading part $F = \dot{F}_c\, t_f - \dot{F}_c(t - t_f - t_h)$ $t_f + t_h < t$	$\sqrt{\frac{\dot{F}_c(2t_f + t_h - t)}{2.22\, E^*}}$	$\sqrt{\frac{\dot{F}_c(4t_f\, t + 2t_h\, t - 2t_h\, t_f - 2t_f^2 - t_h^2 - t^2)}{26.43\, \eta}}$	$\sqrt{\frac{\dot{F}_c\, t_f}{26.43\, H}}$

The viscous part h_{fl} of glass is determined by the assumption of Newtonian flow:

$$\sigma = \eta\, \dot{\varepsilon}\,. \tag{20}$$

Using $\dot{\varepsilon} = \dot{h}_{fl}/h_{fl}$ and $\sigma = F/(c\, h_{fl}^2)$, where $c = 26.43$ is the area constant of the Vickers pyramid, from equation (20) the differential relation between F and h_{fl} follows

$$F = c\, \eta\, h_{fl}\, \dot{h}_{fl}\,. \tag{21}$$

The relation of F and the plastic part h_{pl} is given by the definition of Vickers hardness H:

$$F = c\, H\, h_{pl}^2\,. \tag{22}$$

The solution of the differential equation of this model for different experimental conditions is given in table 1 in the general form $h(t) = h_{el} + h_{fl} + h_{pl}$.

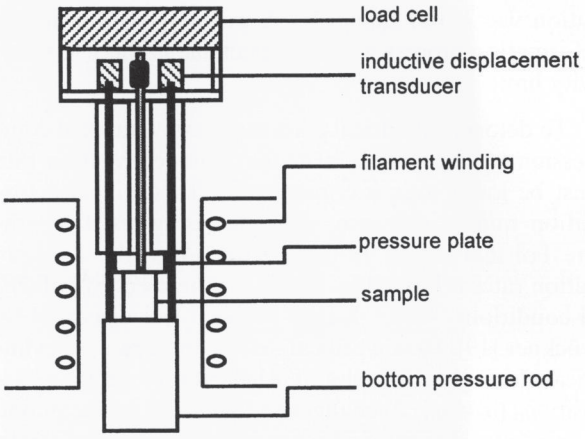

Figure 1. Schematic representation of the special equipment which makes it possible to carry out deformation experiments under different temperature conditions (from room temperature to 600 °C).

3. Experimental

All experiments were performed on commercial sheet glass (T_g = 535 °C, composition (in mol%): 71 SiO_2, 15 Na_2O, 6.6 CaO, 4 MgO, 2 Al_2O_3, 0.9 K_2O, 0.4 SO_3, 0.1 Fe_2O_3). The diameter and the height of the samples for the cylinder compression experiments were 5.6 and 7.5 mm, respectively. The indentation experiments with spherical and pyramidal indenters were performed on (20 × 20 × 7.5) mm^3 plates. After the cutting the samples were tempered at 535 °C for over 3 h to anneal the mechanical and thermal stresses. The samples were cooled down to room temperature at 1 K/min. Before starting the deformation experiments above room temperature the samples were stored once more for 1 h at the deformation temperature.

For the deformation experiments the servo-hydraulic material testing system MTS® 810 (MTS Systems Corporation, Minneapolis, MN (USA)) was used. The different temperature conditions in a range from room temperature to 600 °C were realized by an additional home-built equipment (see figure 1). A special feature of this equipment is the possibility to measure the real time dependences of the temperature $T(t)$ and the deformation parameter $h(t)$, respectively, directly and simultaneously at the sample during the deformation experiment. So it was possible to control the deformation process by the real strain and indentation depth, respectively. For that reason it was not necessary to know a correction function to eliminate the part of deformation of the testing system. The accuracy of the sample temperature regis-

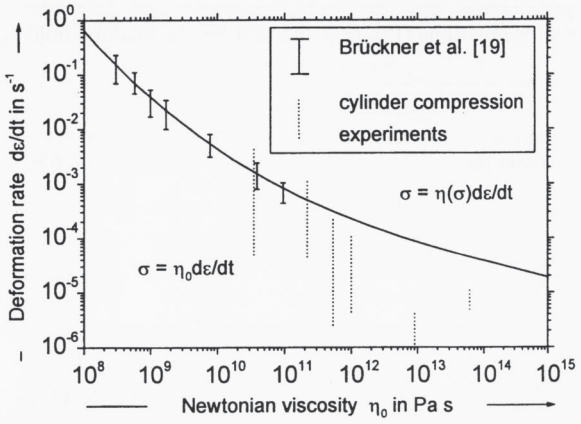

Figure 2. Range of strain rate which was used in this work (dotted line) added to the critical deformation rate for cylindrical float glass samples at which the Newtonian viscosity changes to non-Newtonian viscosity (solid line) given in [19].

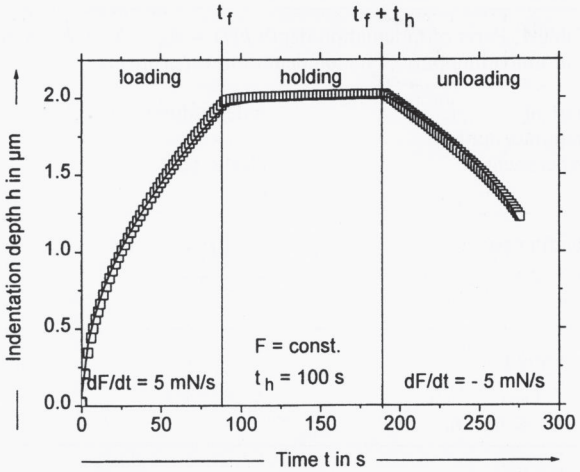

Figure 3. Experimental points and the fitting curve in accordance with table 1 of a single nanoindentation experiment at room temperature.

tration was better than 1 K. A warming-up during the deformation process was not detectable in the 1 K sensitivity limit.

To deform cylindrical glass samples by uniaxial compression without crack formation, the deformation rate must be lower than a critical value. This critical deformation rate is increasing with increasing test temperature. For that reason the temperature for workable deformation rates is limited by 480 °C for the used experimental conditions. An analogous problem was discussed by Brückner [19]. Here a critical deformation rate for cylindrical float glass samples at which the Newtonian viscosity η_0 ($\sigma = \eta_0 \cdot \dot{\varepsilon}$) changes to the non-Newtonian one ($\sigma = \eta(\sigma) \cdot \dot{\varepsilon}$) is given. In figure 2 the ranges of strain rates, which were used in this work, are ascribed to the dependency given in [19].

Two types of experiments were performed by the cylinder compression method. The first experiment was made according to the principle of a parallel plate viscometer. The cylindrical glass samples were deformed with constant strain rate realized by constant deformation rate $\dot{l} = \mathrm{d}l/\mathrm{d}t$, where l is the current length of the cylinder, as long as the purely viscous deformation was reached when the stress persisted constant during deformation. At time $t = t_\mathrm{f}$ the second type of experiment was started (relaxation part) determined by a zero deformation rate $\dot{l}(t) = 0$, that means the sample length will be constant. These types of experiments were performed in the temperature range from 480 to 580 °C.

The home-built equipment for temperature-dependent deformation experiments is constructed in a way that it is very easy to replace the upper pressure plate by indenters of any geometrical shapes. For this work a spherical indenter (radius $R = 1.5$ mm) made of tungsten carbide (Young's modulus $E = 830$ GPa) was used. This material is qualified for indentation experiments up to 600 °C because of high temperature durability. Also two types of indentation modes with spherical indenter were performed. First creep experiments were realized with constant load. The practicability of a preselected load depends on the test temperature. If the temperature is too high the creeping process is too fast, and if the temperature is too low the indentation depth is too small for reliably recording in workable test time. The suitable loads were found from 100 up to 720 N for the used test temperature range from 580 to 400 °C. For these experiments the viscosity η was calculated by equation (8). To obtain more information from the indentation test, a second type was performed composed of the two parts of deformation according to the uniaxial cylinder compression. After the loading part with constant rate of indentation depth ($\dot{h} = \mathrm{d}h/\mathrm{d}t = \dot{h}_\mathrm{c} = \text{const}$) up to a maximum load $F_\mathrm{max} = 400$ N, a holding part with constant indentation depth ($h = h(F_\mathrm{max}) = h_\mathrm{c} = \text{const}$) was followed to be commensurate with the temperature-dependent loading time. From the data of these experiments the viscosity parameter was calculated by equations (17) and (18).

The nanoindentation experiments were realized with help of a NanoIndenter®II using a pyramidal diamond indenter (Vickers). For technical reason, especially the thermal drift, it was not possible to implement indents at temperatures other than room temperature. The regime of the tests was composed of three parts: a loading part with constant loading rate $\dot{F} = \mathrm{d}F/\mathrm{d}t = \dot{F}_\mathrm{c} = \text{const}$ up to a maximum load $F_\mathrm{max} = 450$ mN, a holding part with constant load $F = F_\mathrm{max} = \text{const}$ like an indentation creep experiment for a holding time $t_\mathrm{h} = 100$ s, and an unloading part with the same absolute value of rate as that for the loading part, respectively (see figure 3). Six different loading rates (1 mN/s $\leq \dot{F}_\mathrm{c} \leq$ 50 mN/s) were used. All records of the single indentation experiments (ten indents per loading rate) of this mode were analysed

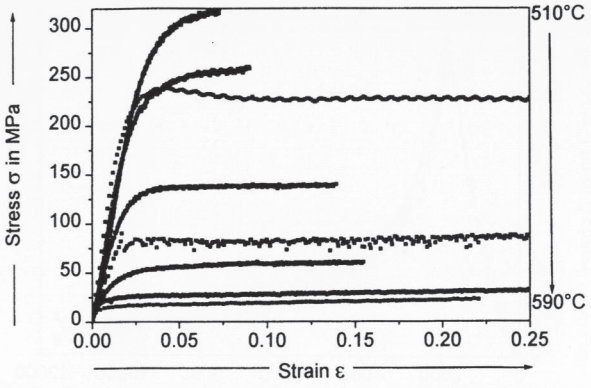

Figure 4. Measured stress-strain curves of cylinder compression experiments for different test temperatures which were carried out at constant strain rate.

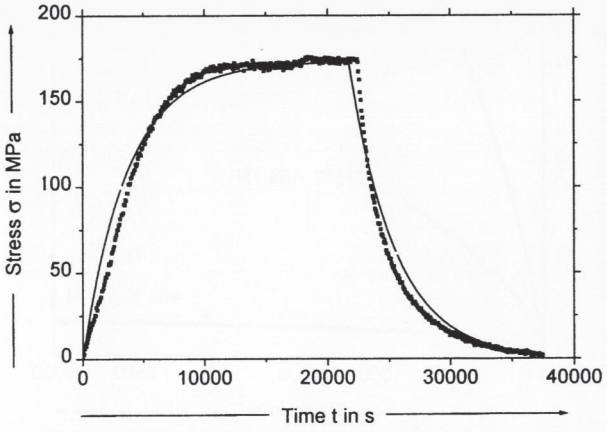

Figure 5. Experimental points and the fitting curve in accordance with equations (6) and (7) of a single cylinder compression experiment with constant strain rate loading and relaxation at 520 °C.

for an indentation depth $h_{lim} \geq 10$ nm to exclude inaccuracies of data near the contact point. In this manner the parameter of viscosity η was calculated in accordance with the solutions of the differential equation of the model given in table 1 for every single indent.

4. Results and discussion

4.1 Cylinder compression experiments

In figure 4 some stress-strain curves of cylinder compression experiments of constant strain rate deformations for different test temperatures are shown exemplarily. If the stress is constant during the increase of the strain ($d\sigma/d\varepsilon = 0$), a pure viscous flow is reached. For this part of deformation a viscosity parameter η was calculated by equation (3). The data points of the stress-strain dependence of a single deformation with both parts, a constant strain rate loading and a relaxation (constant strain) experiment at 520 °C and the fitting curve in accordance with equations (6) and (7) to determine the viscosity parameter are shown in figure 5. It must be pointed out that the rheological fitting parameters are determined by a unified fitting procedure for the complete experiment in reversing to the consistence of the different parts. So it is remarkable that the nonlinear least squares fitting procedure determined the elastic parameter E_H of the single Hookean element of the Zener-Maxwell standard model (see equation (5)) to $E_H \approx 0$ for all measurements at any temperatures which was used. That means the compression of cylindrical glass samples is describable by a simple Maxwell model with a good approximation for this range of temperature. The behaviour of the elastic parameter E_M of the Maxwell model will be discussed in a separate paper [20].

The results of the analysis of the two types of cylinder compression experiment with respect to equation (3)

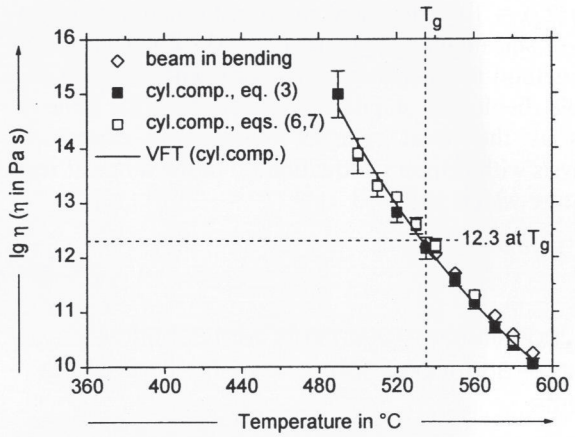

Figure 6. Viscosity parameters of beam in bending experiments and cylinder compression experiments (cyl. comp.) analysed by equation (3) and equations (6) and (7) in dependence on the test temperature. The constants of the Vogel-Fulcher-Tammann (VFT) relation were fitted by the experimental results of the cylinder compression experiments.

and equations (6) and (7), respectively, relating to the viscosity parameters, are shown in figure 6 in dependence on temperature. The parameters of the VFT equation (1) were fitted to $A = 0.652$, $B = 2868.7$ °C, and $T_0 = 286.5$ °C. The corresponding fitting curve is drawn in figure 6 additionally. Furthermore the results of standard viscosity measurements by beam in bending method for the same sheet glass are shown in figure 6. The reflection of these results impressively shows the very good agreement between the values of viscosity received by the different experimental methods and different methods of analysing the measured data. Moreover both the values of viscosity and the line of the VFT relation are very near to the point of intersection defined

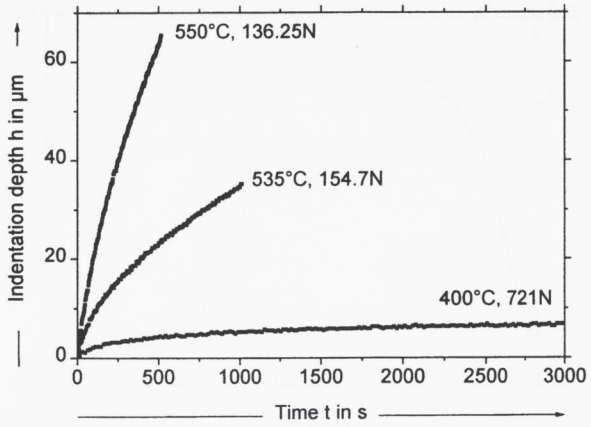

Figure 7. Experimental points of indentation creep experiments with a spherical indenter (radius R = 1.5 mm) performed at different temperatures and different maximum loads consequently.

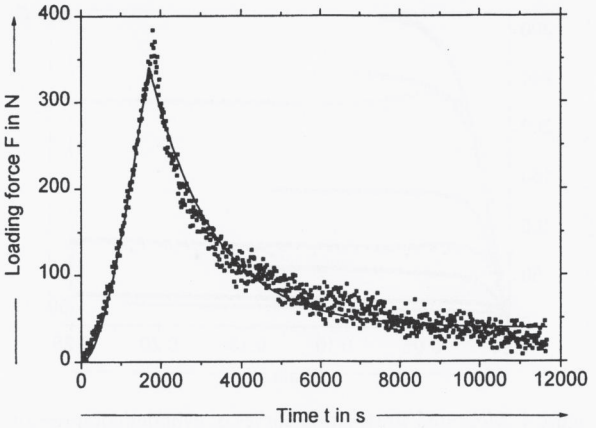

Figure 8. Experimental points and the fitting curve in accordance with equations (16) and (18) of a single ball indentation experiment (R = 1.5 mm) with loading at constant displacement rate and relaxation.

by $\eta(T_g) = 10^{12.3}$ Pa s and the transformation temperature of silicate glass T_g (here T_g = 535 °C). That means the method to calculate the viscosity with the help of a simple rheological standard model leads to the same results as the usual cylinder compression experiment analysis with respect to equation (3) in the range of temperature which was used.

4.2 Indentation experiments with spherical indenter and topographical investigations of the indents

Three examples of indentation depth-time dependences of indentation creep experiments with spherical indenter by three different temperatures and hence by different maximum loads are shown in figure 7. This type of test was performed in a range from 400 to 580 °C. The conventionally viscosity parameters were calculated by equation (8). In figure 8 the measurement points of the load-time dependence of a single indentation experiment, once more with a loading part ($\dot{h} = \dot{h}_c$ = const) and a relaxation part ($h = h_c$ = const), are shown to exemplify tests, which were analysed by rheological principles in accordance with equations (16) and (18). The constant Γ_s (see equation (17)) was fixed to Γ_s = 4/3 for all these experiments, neglecting the temperature dependence of the Poisson ratio ν. In the same manner as the cylinder compression experiments the fitting procedure determined $E_H \approx 0$ for all measurements.

In figure 9 the temperature dependence of viscosity is compared for all indentation experiments together with the VFT relation from figure 6. The agreement between the classical values of viscosity determined by equation (8) and the rheological parameters fitted by equations (16) and (18) is not so excellent as shown before in figure 6 for cylinder compression experiments. On the other hand, the two different indentation rates $\dot{h}$ = 0.033 µm/s and $\dot{h}$ = 0.333 µm/s, respectively, yield no significant differences of values of viscosity for rheological calculation in accordance with the theoretical expectance. The tendency for the viscosity to increase with decreasing temperature will be smaller and the ball viscosity will not exceed 10^{16} Pa s up to 400 °C, respectively. This behaviour is strongly in contrast to the extrapolation of the VFT equation (1) yielding a steady increase of the viscosity with decreasing temperature up to infinity at T_0 = 286.5 °C, which is remarkable in principle.

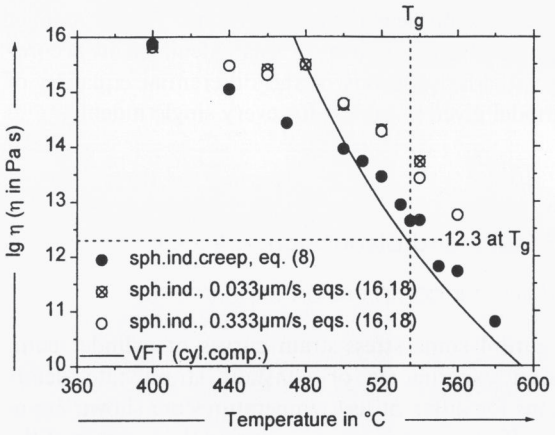

Figure 9. Viscosity parameters of indentation creep experiments (sph. ind. creep) calculated by equation (8) and indentation experiments (sph. ind.) with spherical indenter (R = 1.5 mm) analysed by equations (16) and (18) in dependence on the test temperature. The constants of the Vogel-Fulcher-Tammann (VFT) relation were fitted by the experimental results of the cylinder compression experiments.

A very interesting result about the ball indentation experiments follows from the profile records of the in-

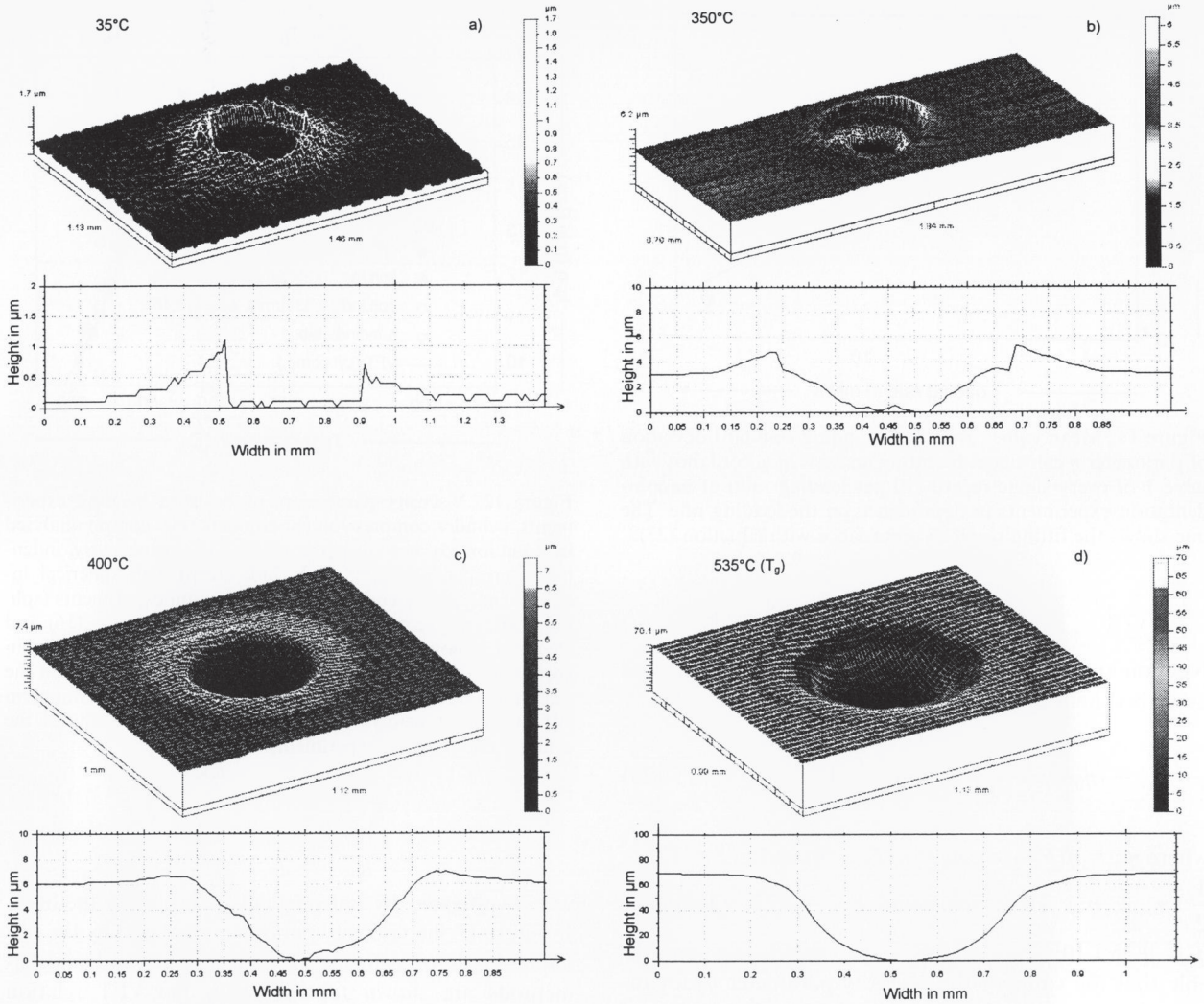

Figures 10a to d. Profile records (top) and single scan lines (bottom) of indents carried out with spherical indenter (R = 1.5 mm) at 23 °C (figure a), 350 °C (figure b), 400 °C (figure c) and T_g = 535 °C (figure d).

dents performed at different typical temperatures (see figures 10a to d). At room temperature (23 °C, figure 10a) the height of the indent after unloading is on the same level as the sample surface in accordance with the data of loading/unloading curves, which shows negligible hysteresis. But around the indent palisades like ridges of about 2 µm height are visible in the region of the Hertzian ring fractures. Up to 350 °C distortions like craters are detectable inside the Hertzian ring fractures as well as some hysteresis effects in the loading/unloading behaviour. In the future more detailed investigations will be carried out to qualify this first impression. At 350 °C characteristic viscoelastic piling up is observed. From 400 °C onward a transition to sinking in is visible (see figures 10b to d) indicating the dominance of the purely viscous deformation process. Therefore it is also probable that the real contact area between sample and indenter has not yet the same relation to the indentation depth for all test temperatures. The aim of future work will be to obtain more information about the real contact area by analysis of profile records.

4.3 Nanoindentation experiments

All of the nanoindentation experiments were realized at room temperature. For every constant load rate varying from $\dot{F}$ = 1 mN/s to $\dot{F}$ = 50 mN/s ten indents were performed and analysed by the equations of table 1. An example of the results of the fitting procedure is shown in figure 3 by the curves, calculated by the fitting parameters. In figure 11 the mean values of the viscosity parameters are shown in dependence on the loading rate. The transition from viscosities of very small loading rates to viscosities of higher loading rates, which was identified by Yue and Brückner [21] as a transition from

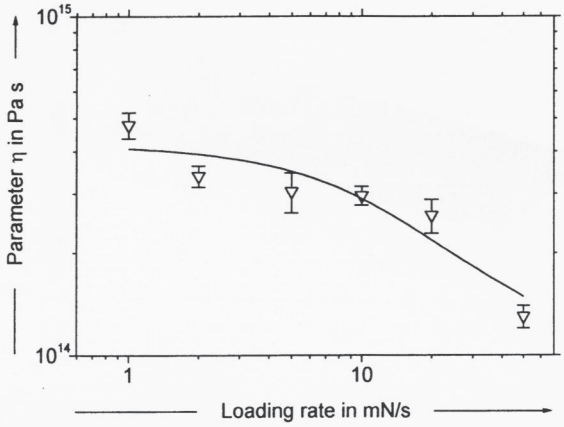

Figure 11. Mean values and corresponding standard deviation of parameter η calculated by fitting analysis in accordance with table 1 of every single record (10 per loading rate) of nanoindentation experiments in dependence on the loading rate. The line shows the fitting result in accordance with equation (23).

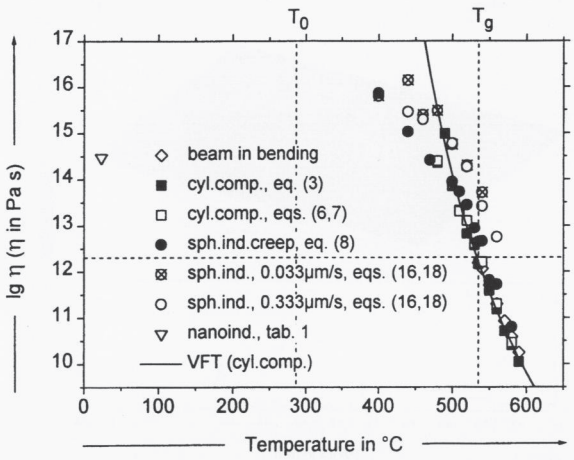

Figure 12. Viscosity parameters of beam in bending experiments, cylinder compression experiments (cyl. comp.) analysed by equation (3) and equations (6) and (7), respectively, indentation creep experiments (sph. ind. creep) with spherical indenter analysed by equation (8), indentation experiments (sph. ind.) with the same indenter analysed by equations (16) and (18) and nanoindentation experiments (nanoind.) analysed in accordance with the equations of table 1 in dependence on the test temperature. The constants of the Vogel-Fulcher-Tammann (VFT) relation were fitted by the experimental results of the cylinder compression experiments.

Newtonian viscosity η_0 to Binghamian viscosity η_∞, was described here by

$$\eta = \eta_\infty + (\eta_0 - \eta_\infty) \cdot \frac{2}{\pi} \cdot \arctan\left(\frac{\dot{F}}{\dot{F}_g}\right) \qquad (23)$$

where $\eta_\infty = \eta(\dot{F} \to \infty)$, $\eta_0 = \eta(\dot{F} \to 0)$, and $\eta(\dot{F} = \dot{F}_g) = \frac{1}{2}(\eta_0 + \eta_\infty)$. Here are found $\eta_\infty = 4.22 \cdot 10^{14}$ Pa s, $\eta_0 = 9.25 \cdot 10^{13}$ Pa s, and $\dot{F}_g = 13.7$ mN/s. It is remarkable that the value of the viscosity parameter η_0 for infinitesimal loading rates is smaller by over five orders of magnitude than the fictive values for the viscosity of glasses at room temperature in [5] ($\eta_{RT} \approx 10^{20}$ Pa s) and [6] ($\eta_{RT} \approx 10^{40}$ Pa s). On the other hand, the range of investigated loading rates is too small for a reliable extrapolation. However, the decrease of the viscosity parameter η with increasing loading rate $\dot{F}$ is undisputed and also was shown for the optical glass BK7 and for the polymer PMMA in [7]. A first idea about the physical reason for this dependence is that a part of the mechanical energy input during the indentation process is converted into thermal energy and so the temperature is increasing and, in turn, the viscosity is decreasing for a local volume of the glass sample deformed under the indenter. To calculate the increase of the temperature during indentation accurately, it is necessary to know the real volume of the glass sample that is involved in this process. But this problem is not cleared up completely up to now.

5. Summary and conclusions

The temperature dependence of the viscosity of commercial sheet glass below the transformation temperature was investigated by independent deformation methods. In figure 12 the viscosity parameters obtaind by the different kinds of deformation experiments and analysis methods are shown together with the VFT relation which is a result of measurement according to a parallel plate viscometer. The results of the different methods of calculation of the viscosity parameters for the cylinder compression experiments shows a good accordance with the results of measurements by beam in bending method in the used range of temperature. That means the analysis by rheological principles is applicable to cylinder compression experiments. Moreover, it could be shown that for the calculation a simple Maxwell model is to be prefered because the fitting procedure leads to an Hookean elastic parameter $E_H \approx 0$ for every data set if a standard Zener-Maxwell model was used. The temperature dependence of the Hookean parameter E_M of the consequently used Maxwell model will be discussed in a future work [20].

The accordance between the results of indentation creep experiments with a spherical indenter and the VFT relation, the results of cylinder compression and the beam in bending experiments, respectively, is very impressive up to 500 °C (T_g = 535 °C). Lower than 500 up to 400 °C it could be shown by topographical investigations of any ball indents that the mechanism of deformation is dominated by viscous flow indeed and that the measured values of viscosity are many times smaller than the phenomenological VFT values at this tempera-

ture range. The values of the rheological analysis, which was based on the same model as was used for the uniaxial cylinder compression experiments, indicate a similar course of the viscosity parameters. The good agreement between the rheological parameters of the different displacement rates $\dot{h}$ explains the sufficient consideration of the deformation rate in the model.

A partial result of this work is that it is possible to analyse nanoindentation experiments with sharp indenters by rheological principles in continuation of [22]. But the dependence of the viscosity parameters from the deformation rate must be cleared up more exactly in future. Primarily the gap of viscosity values from room temperature to 400 °C (see figure 12) must be investigated. To vary the pressure and stress, respectively, indentation experiments with different indenter geometry are appropriate in a range from room temperature to transformation temperature of glass.

6. List of symbols

A, B, T_0	constants of Vogel-Fulcher-Tammann equation (1)
A_0	cross section of the cylindric samples at $t = 0$
a	contact radius
C_G	numeric constant of pyramidal indenter
c	area constant of pyramidal indenter
E	elastic modulus
E^*	reduced elastic modulus
E_H	elastic parameter of single Hookean element of Zener-Maxwell model
E_M	elastic parameter of Hookean element of Maxwellian section of Zener-Maxwell model
F	loading force
F_f	loading force at $t = t_f$
F_∞	loading force at $t \to \infty$
F_{max}	maximum load
$\dot{F}$	loading rate (= dF/dt)
$\dot{F}_c$	constant loading rate
$\dot{F}_g$	half-value loading rate (equation (23))
H	hardness
h	indentation depth
h_{el}	elastic part of indentation depth
h_f	indentation depth at $t = t_f$
h_{fl}	viscous (flow) part of indentation depth
h_{lim}	lower limit of nanoindentation depth for analysis
h_{pl}	plastic part of indentation depth
$\dot{h}$	indentation rate (= dh/dt)
$\dot{h}_c$	constant indentation rate
l	actual length of cylindric samples
l_0	length of cylindric samples at $t = 0$
$\dot{l}$	axial deformation rate of cylindric samples (= dl/dt)
m_s	geometric constant of the deformation process with spherical indenter
r	radius of cylindric sample
R	radius of spherical indenter
RT	room temperature
t	time
t_f	duration time of the loading process
t_h	duration time of the holding process
T	temperature
T_g	transformation temperature
V	volume of cylindric samples
Γ	material constant
Γ_s	prefactor of the solution $F(t)$ for deformation by spherical indenter
ε	strain
ε_f	strain at $t = t_f$
$\dot{\varepsilon}$	strain rate (= $d\varepsilon/dt$)
$\dot{\varepsilon}_c$	constant strain rate
η	viscosity
η_{RT}	viscosity at room temperature
η_0	Newtonian viscosity
η_∞	Binghamian viscosity
ν	Poisson ratio
σ	stress
σ_f	stress at $t = t_f$
σ_∞	stress at $t \to \infty$
$\dot{\sigma}$	stress rate (= $d\sigma/dt$)
τ	relaxation time
$\Psi(t)$	viscoelastic function

*

The authors thank the Deutsche Forschungsgemeinschaft, Bonn-Bad Godesberg (project no. Gr. 1482/1-2) and the Kultusministerium of Sachsen-Anhalt (project no. 2158A/0085B) for sponsoring parts of this work. Furthermore, the authors would like to express their thanks to the Institut für Neue Materialien, Saarbrücken (head: Prof. Dr. H. Schmidt), for measurements by the beam in bending method and to Dipl.-Phys. Kanina Neideck for taking indentation experiments with spherical indenter.

7. References

[1] Tammann, G.: Der Glaszustand. Leipzig: Voss, 1933.
[2] Vogel, H.: Das Temperaturabhängigkeitsgesetz der Viskosität von Flüssigkeiten. Physik. Z. **22** (1921) p. 645–646.
[3] Fulcher, G. S.: Analysis of recent measurements of the viscosity of glasses. J. Am. Ceram. Soc. **8** (1925) Pt. 1, no. 6, p. 339–355; Pt. II, no. 12, p. 789–794.
[4] Tammann, G.; Hesse, W.: Die Abhängigkeit der Viskosität von der Temperatur bei unterkühlten Flüssigkeiten. Z. anorg. allg. Chem. **156** (1926) p. 245–257.
[5] Frischat, G. H.: Glas – Struktur und Eigenschaften. In: Lohmeyer, S. et al. (eds.): Werkstoff Glas I. Ehningen: expert, 1987. p. 47–67.
[6] Macosco, C. W.: Rheology – principles, measurements and applications. New York et al.: VCH, 1994.
[7] Meinhard, H.: Rheologische Untersuchungen zu Härteeindruckexperimenten im Nanometerbereich. Univ. Halle, Diss. 1999.
[8] Douglas, R. W.; Armstrong, W. L.; Edward, J. P. et al.: A penetration viscometer. Glass Technol. **6** (1965) no. 2, p. 52–55.
[9] Brückner, R.; Demharter, G.: Systematische Untersuchung über die Anwendbarkeit von Penetrationsviskosimetern. Glastechn. Ber. **48** (1975) no. 1, p. 12–18.
[10] Gent, A. N.: Theory of the parallel plate viscometer. Brit. J. Appl. Phys. **11** (1960) p. 85–87.
[11] Brückner, R.; Yue, Y.; Habeck, A.: Determination of the rheological properties of high-viscous glass melts by the cylinder compression method. Glastech. Ber. Glass Sci. Technol. **67** (1994) no. 5, p. 114–129.
[12] Hertz, H.: Über die Berührung fester elastischer Körper. J. reine angew. Math. **92** (1881) p. 156–171.
[13] Tabor, D.: Indentation hardness: Fifty years on; a personal view. Phil. Mag. A **74** (1996) no. 5, p. 1207–1212.
[14] Graham, G. A. C.: The contact problem in the linear theory of viscoelasticity. Int. J. Engng Sci. **3** (1965) p. 27–46.

[15] Lee, E. H.; Radok, J. R. M.: The contact problem for viscoelastic bodies. J. appl. Mech. **27** (1960) p. 438–444.
[16] Brückner, R.; Yue, Y.; Deubener, J.: Progress in the rheology of glass melts – A survey. Glastech. Ber. Glass Sci. Technol. **70** (1997) no. 9, p. 261–271.
[17] Sneddon, I. N.: The relation between load and penetration in the axisymmetric Boussinesq problem for a punch of arbitrary profile. Int. J. Engng Sci. **3** (1965) p. 47–57.
[18] Murakami, Y.; Tanaka, K.; Itokazu, M. et al.: Elastic analysis of triangular pyramidal indentation by the finite-element method and its application to nanoindentation measurement of glasses. Phil. Mag. A **69** (1994) no. 6, p. 1131–1153.
[19] Brückner, R.; Yue, Y.: Non-Newtonian flow behaviour of glass melts as a consequence of viscoelasticity and anisotropic flow. J. Non-Cryst. Solids **175** (1994) p. 118–128.
[20] Meinhard, H.; Fränzel, W.; Grau, P.; Berg, G.: Mechanische Eigenschaften von Glas unter hohen Drücken. Reported at 74th Meeting of the German Society of Glass Technology (DGG) in Ulm (Germany) on 30 May 2000.
[21] Yue, Y.; Brückner, R.: Comparison of some non-Newtonian flow equations for inorganic glass melts and amorphous polymers. J. Non-Cryst. Solids **202** (1996) p. 253–265.
[22] Grau, P.; Berg, G.; Meinhard, H. et al.: Strain rate dependence of the hardness of glass and Meyer's law. J. Am. Ceram. Soc. **81** (1998) no. 6, p. 1557–1564.

0101P002

Address of the authors:

H. Meinhard, W. Fränzel, P. Grau
Martin-Luther-Universität
Halle-Wittenberg
Fachbereich Physik
Friedemann-Bach-Platz 6
D-06108 Halle/Saale (Germany)
e-mail: meinhard@physik.uni-halle.de